Dynamic modelling of green algae cultivation in a photobioreactor for sustainable biodiesel production

Ehecatl Antonio del Rio-Chanona[3,4,‡], Jiao Liu[1,2,‡], Jonathan L. Wagner[4], Dongda Zhang[3,4*], Yingying, Meng[1,2], Song Xue[1,*], Nilay Shah[3,4]

1: Marine Bioengineering Group, Dalian Institute of Chemical Physics, Chinese Academy of Sciences, Dalian 16023, China

2: University of Chinese Academy of Sciences, Beijing 100049, China

3: Centre for Process Systems Engineering, Imperial College London, South Kensington Campus, London SW7 2AZ, UK

4: Department of Chemical Engineering, Imperial College London, South Kensington Campus, London SW7 2AZ, UK.

‡: These authors contributed equally to this work.

*: corresponding authors, email: dz1510@ic.ac.uk (Dongda Zhang), tel: 44 (0)7543 785283; email: xuesong@dicp.ac.cn (Song Xue), tel: 86 411 84379069.

Running title: Kinetic Modelling of Algal Biodiesel Production

Abstract

Biodiesel produced from microalgae has been extensively studied due to its potentially outstanding advantages over traditional transportation fuels. In order to facilitate its industrialisation and improve the process profitability, it is vital to construct highly accurate models capable of predicting the complex behaviour of the investigated biosystem for process optimisation and control, which forms the current research goal. Three original contributions are described in this paper. Firstly, a dynamic model is constructed to simulate the complicated effect of light intensity, nutrient supply and light attenuation on both biomass growth and biolipid production. Secondly, chlorophyll fluorescence, an instantly measurable variable and indicator of photosynthetic activity, is embedded into the model to monitor and update model accuracy especially for the purpose of future process optimal control, and its correlation between intracellular nitrogen content is quantified, which to the best of our knowledge has never been addressed so far. Thirdly, a thorough experimental verification is conducted under different scenarios including both continuous illumination and light/dark cycle conditions to testify the model predictive capability particularly for long-term operation, and it is concluded that the current model is characterised by a high level of predictive capability. Based on the model, the optimal light intensity for algal biomass growth and lipid synthesis is estimated. This work, therefore, paves the way to forward future process design and real-time optimisation.

Keywords: biodiesel production; dynamic modelling; chlorophyll fluorescence; model predictive capability; light/dark cycle; nitrogen limiting.

Introduction

Microalgae are considered to be a promising feedstock for the production of renewable biofuels which would contribute to meeting the ever-increasing global demand for energy (Mata, Martins, and Caetano 2010). Compared to plant-based biofuel precursors, including both food crops such as corn or sugarcane and non-food plants, *e.g.* jatropha, microalgae display superior growth rates and shorter generation time, can utilise wastewater as a nutrient source, do not compete for arable land with food crops, and are expected to have low environmental impacts *etc.* (Sheehan et al. 1998; Schenk et al. 2008; Brennan and Owende 2010). Furthermore, the metabolic reaction networks in microalgae have been extensively researched over the last decades, resulting in the successful identification and genetic modification of a variety of microalgae species capable of synthesising different sustainable biofuels including biodiesel, bioethanol, biohydrogen, bioisoprene, and biohydrocarbons (Adesanya et al. 2014; Matos et al. 2013; Eroglu and Melis 2010).

Amongst these, a major focus has been placed on the production of algal lipid, which can contribute up to 70 wt% of dry cell weight and is readily converted into biodiesel, already used as a fossil fuel substitute (Brennan and Owende 2010; Wen et al. 2016). To facilitate the commercialisation of this process, comprehensive studies have been conducted with the aim to enhance both the biomass growth rate and biolipid productivity. For example, the effects of modifying key operating conditions *e.g.* light intensity, temperature, pH and nutrient supply, have been thoroughly investigated with the conclusion that biolipid synthesis can be remarkably stimulated under nitrogen limiting conditions (Converti et al. 2009; Scott et al. 2010). Different biomass cultivation methods (*e.g.* autotrophic, heterotrophic and mixotrophic) have been widely explored and their respective advantages and limitations have been discussed in detail (S. J. Yoo, Kim, and Lee 2014; Wang et al. 2016; Purkayastha et al. 2017). In addition, recent studies conducted life cycle assessments and process scale-up

experiments which revealed that the biolipid content in large scale processes is often reduced by over 60% (rarely reaching 30 wt%), significantly decreasing the process profitability and rendering it economically unviable at present (Wen et al. 2016; Purkayastha et al. 2017; Park and Li 2015).

To resolve this severe challenge, it is necessary to implement rigorous process control and optimisation regimes, which can achieve dense biomass concentrations as well as high biolipid productivities simultaneously (Bernard, Mairet, and Chachuat 2015; del Rio-Chanona, Zhang, and Vassiliadis 2016). To this end it is crucial to construct highly accurate models capable of simulating the dynamic behaviour of the underlying bioprocess and to identify easily measurable state variables. Meanwhile, developing robust dynamic optimisation algorithms for highly nonlinear biosystems is also regarded an important prerequisite for this work to be accomplished successfully. So far, different models have been developed to simulate the effect of key operating conditions on both microalgae growth and biofuel production (Adesanya et al. 2014; Dongda Zhang et al. 2015; Cakmak et al. 2012). Specific variables including pH, dissolved oxygen, chlorophyll fluorescence (Y(II)) or light irradiation have been used to monitor the process performance and design control schemes (C. Yoo et al. 2015; Keymer, Pratt, and Lant 2013; S. J. Yoo, Kim, and Lee 2014; Bernard, Mairet, and Chachuat 2015). We recently proposed a state-of-the-art real-time optimisation strategy for long-term bioprocess optimisation which incorporates parameter re-estimation into economic model predictive control and was demonstrated to be highly effective compared to traditional offline optimisation methods (del Rio-Chanona, Zhang, and Vassiliadis 2016).

Despite these achievements, it is important to note that the employed models must also have a high predictive capability so that they can accurately determine the optimal operating conditions for biomass growth and biofuel synthesis. In order to effectively implement real-

time process optimisation, it is necessary to embed variables that can be measured instantly (*e.g.* Y(II)), allowing continuous calibration of the model and minimising deviations from experimental or operational data. However, much less effort has been devoted to these areas to date. For instance, whilst mathematical models specific to biolipid synthesis have been proposed in the past, their predictive capabilities have rarely been evaluated. In some cases, it was necessary to use different sets of parameter values when applying the models to simulate different experiments, even if the experiments were conducted under similar conditions. Meanwhile, instantly measurable variables that can reflect biomass growth and biolipid synthesis activities, particularly chlorophyll fluorescence (Y(II)) which is widely used to represent the photosynthetic activity of microalgae cells, have never been included in these models. Thus, these limitations prevent their further application for process optimisation.

Consequently, to close this gap, the present study aims to construct a highly accurate dynamic model suitable for the real-time control and optimisation of a long-term microalgal biodiesel production process. In particular, the instantly measurable variable, chlorophyll fluorescence, will be embedded into the current model, and the model predictive capability will be verified under different operating conditions. Furthermore, the model simulation results will be used to identify the primary limiting factors for biodiesel production.

2. Materials and modelling methodology

2.1 Experiment setup

Nannochloropsis oceanica IMET1 was provided by Dr. Jian Xu from the Qingdao Institute of Bioenergy and Bioprocess Technology, Chinese Academy of Sciences, and maintained in seawater supplemented with modified F/2 medium. The 500 mL bubble column bioreactor (5 cm diameter) was supplied with 100 mL/min of filtered air, supplemented with 2% (v/v) CO_2, as described by Pan et al. (2016). The pre-culture was prepared in the photobioreactor (PBR) with sufficient nutrients and under continuous illumination with white fluorescent light (140

119 μmol m^{-2} s^{-1}) for 4 days, followed by inocculation into new PBRs at an initial biomass
120 concentration of ~0.18 mg mL^{-1}. In total, four batch experiments were carried out with
121 different initial nitrate concentrations and light intensities as shown in Table I, and a constant
122 ambient temperature of 25 ± 1 ºC.

123 **2.2 Analytical methods**

124 Biomass concentrations (mg mL^{-1}) were determined as described previously (Zhu and Lee
125 1997). Cells were harvested by centrifugation and pellets were washed twice with 0.5 M
126 NH_4HCO_3 and dried at 60 ºC to constant weight. Nitrate concentrations in the medium were
127 measured using a UV/VIS spectrophotometer with a pre-drawn standard curve for the nitrate-
128 related light absorption (Chi et al. 2016). The fluorescence parameter Y(II), which reflects the
129 effective photosynthesis capacity of photosynthesis system II, was calculated using a
130 chlorophyll fluorometer (Water-PAM WALZ, Germany) based on the method described by
131 Yao et al. (2012). Light intensity was measured on an Optometer P9710 with a
132 photosynthetically active radiation detector (Gigahertz Optik Corporation, Germany).
133 Biomass intracellular nitrogen content was determined using an elemental analyser (Vario EL
134 cube, Elementar Analysensysteme GmbH Germany). The yields of the transesterified fatty
135 acid methyl esters (FAMEs) were quantified by gas chromatography using the internal
136 standard glyceryl triheptadecanoate (Liu et al. 2015).

137 **2.2 Model construction**

138 In order to construct an accurate dynamic model, an understanding of the underlying kinetic
139 mechansims is essential. The synthesis of the biolipid fraction is mediated by the intracellular
140 nitrogen concentration (nitrogen quota) and sufficiency in light intensity, and its production is
141 dependent on the biomass concentration which is affected by the nitrate concentration in the
142 culture (Li et al. 2008; Scott et al. 2010). Therefore, all of these variables should be included.

Furthermore, *chlorophyll fluorescence (Y(II))* is also embedded into the dynamic model due to its importance for future real-time process monitor and control.

2.2.1 Algal biomass growth

Eq. 1 is commonly used to estimate the algal biomass growth rate. The first term on the right represents biomass growth, whilst the second term represents biomass decay. Previous research concluded that the specific biomass growth rate (μ_0) depends on both light intensity and nitrate concentration, whilst the biomass decay rate (μ_d) is a function of temperature only (D. Zhang et al. 2015). As the temperature was fixed in this study, μ_d reduces to a constant. To model the effect of nitrate concentration on biomass growth, the Droop model was Eq. 2, as it is predominantly applied under nutrient limiting conditions (del Rio-Chanona et al. 2017; Adesanya et al. 2014).

$$\frac{dX}{dt} = \mu_0 \cdot X - \mu_d \cdot X \quad (1)$$

$$\mu_0 = \mu_m(I) \cdot \left(1 - \frac{k_q}{q}\right) \quad (2)$$

where X is biomass concentration (g L^{-1}), u_0 is specific growth rate (h^{-1}), u_d is specific decay rate (h^{-1}), $u_m(I)$ denotes the effect of light intensity (I) on biomass growth, k_q is minimum nitrogen quota (mg g^{-1}), and q is nitrogen quota (mg g^{-1}).

2.2.2 Nitrate consumption

Whilst nitrates are essential for biomass growth, high nitrate concentrations can severely supress the accumulation of biolipid (Mata, Martins, and Caetano 2010). Consequently, the nitrate consumption rate was modelled using an adopted form of the the Monod model (Eq. 3), commonly used to simulate nutrient consumption (Dongda Zhang et al. 2016; Fouchard et al. 2009).

$$\frac{dN}{dt} = -\mu_N \cdot \frac{N}{N + K_N} \cdot X \quad (3)$$

where N is culture nitrate concentration (mg L^{-1}), K_N is half-velocity coefficient (mg L^{-1}), and u_N is maximum specific nitrate uptake rate (mg g^{-1} h^{-1}).

2.2.3 Nitrogen quota

Intracellular nitrogen content, also termed nitrogen quota, is one of the key variables and predominantly determines both biomass growth and biolipid synthesis. Previous research has concluded that higher nitrogen quota can result in a higher biomass growth rates, whilst lower nitrogen quota can stimulate the synthesis of biolipid (Sharma, Schuhmann, and Schenk 2012). As nitrate is only consumed by algal cells, based on a mass balance, the nitrate consumption rate must be equal to the accumulation of intracellular nitrogen (Eq. 4). This equation can then be transformed to Eq. 5, to calculate the accumulation rate of nitrogen quota.

$$\frac{d(X \cdot q)}{dt} = -\frac{dN}{dt} = \mu_N \cdot \frac{N}{N + K_N} \cdot X \tag{4}$$

$$\frac{dq}{dt} = \mu_N \cdot \frac{N}{N + K_N} - \mu_m(I) \cdot \left(1 - \frac{k_q}{q}\right) \cdot q \tag{5}$$

2.2.4 Fatty acid methyl ester (FAME) production

The kinetic mechanism of biolipid (fatty acids) synthesis has been illustrated in recent works (Gnansounou and Raman 2016). It is demonstrated that all the CO_2 fixed through photosynthesis is converted to sugar initially. Then, a portion of sugar is converted into fatty acids, and this reaction rate is proportional to the nitrogen quota. Meanwhile, fatty acids can also be consumed to produce functional carbon molecules (*e.g.* membranes), of which the reaction rate increases with the increasing nitrate uptake rate. Inspired from this mechanism, Eq. 6 is constructed in this study to simulate total fatty acid production ($X \cdot S$). This equation is then transformed to Eq. 7 to simulate the accumulation rate of intracellular fatty acid (S).

$$\frac{d(X \cdot S)}{dt} = (\theta' \cdot q) \cdot \mu_m(I) \cdot \left(1 - \frac{k_q}{q}\right) \cdot X - \gamma' \cdot \mu_N \cdot \frac{N}{N + K_N} \cdot X \tag{6}$$

$$\frac{dS}{dt} = \mu_m(I) \cdot (\theta' \cdot q - S) \cdot \left(1 - \frac{k_q}{q}\right) - \gamma' \cdot \mu_N \cdot \frac{N}{N + K_N} \quad (7)$$

where θ' and γ' are kinetic constants for biolipid synthesis and consumption, respectively, and S is intracellular fatty acids content (wt%).

Moreover, since the current study aims to simulate biodiesel production, FAMEs rather than fatty acids are chosen for model construction. The benefit of modelling FAME production instead of lipid content in cells is that FAME is the final product – *biodiesel*. Therefore, in the current study, FAME production after lipid transesterification was measured directly and described in Section 2.2. Because FAME comes from biolipid through transesterification, its synthesis rate can be approximated by modifying Eq. 7 into Eq. 8 (Gnansounou and Raman 2016).

$$\frac{df}{dt} = \mu_m(I) \cdot (\theta \cdot q - \varepsilon \cdot f) \cdot \left(1 - \frac{k_q}{q}\right) - \gamma \cdot \mu_N \cdot \frac{N}{N + K_N} \quad (8)$$

where θ, γ, and ε are modified parameters taking into account the complex effects of lipid synthesis and transesterification conversion, and f is FAME yield (wt%).

2.2.5 Chlorophyll fluorescence (Y(II))

Chlorophyll fluorescence (Y(II)) is used to estimate the efficiency of the microalgal Photosystem II (PSII), as it represents the ability of microalgae to use absorbed quanta and gives a realistic reflection of the physiological state of microalgae cells. Whilst the biolipid synthesis is not directly linked to the status of YII), it provides a precise reflection in the change of nitrogen quota and is highly consistent with biolipid accumulation. Therefore, it is vital to embed Y(II) into the current model, so that it can be used to monitor model deviations and calibrate the model for future real-time process optimisation using instant chlorophyll fluorescence measurements.

To date, no research has quantified the correlation between Y(II) and nitrogen quota. Nonetheless, it was found that an exponential relationship between photosynthesis rate and

chlorophyll content exists in algae (Béchet, Shilton, and Guieysse 2013). As Y(II) represents the efficiency of PSII which is directly related to photosynthesis rate and the nitrogen quota can have a notable effect on the intracellular chlorophyll content (Li et al. 2008), it is proposed to use Eq. 9 to simulate the change of Y(II) with respect to nitrogen quota.

$$\mathrm{Y(II)} = \frac{\exp[\tau \cdot q]}{\exp[\tau \cdot q] + \delta} + \varphi \tag{9}$$

where τ, δ and φ are kinetic parameters in this equation.

2.2.6 Simulation of light intensity

The effect of light intensity on biomass growth has been well studied and is commonly simulated by the Aiba model (Eq. 10) (Béchet, Shilton, and Guieysse 2013). Furthermore, photons in a PBR are either absorbed by microalgal biomass or scattered by bubbles, causing the local light intensity to diminish along the light transmission direction in the reactor. To take this light attenuation into account, a modified form of the Lambert-Beer law has been proposed and has been widely utilised in recent studies, as shown in Eq. 11 (Dongda Zhang et al. 2016).

$$u_m(I) = u_M \cdot \frac{I}{I + k_s + \frac{I^2}{k_i}} \tag{10}$$

$$I(z) = I_0 \cdot \exp[-(\alpha \cdot X + \beta) \cdot z] \tag{11}$$

where u_M is maximum specific growth rate (h^{-1}), I is light intensity (μmol m^{-2} s^{-1}), k_s and k_i are light saturation term (μmol m^{-2} s^{-1}) and light inhibition term (μmol m^{-2} s^{-1}) for cell growth, respectively, I_0 is incident light intensity (μmol m^{-2} s^{-1}), α is cell absorption coefficient (m^2 g^{-1}), β is bubble scattering coefficient (m^{-1}), z is the distance from light source (m), and L is the width of the PBR (m).

However, when adding light attenuation into the current model, the model complexity is significantly increased due to the presence of both spatial and temporal dimensions. Thus, in

order to simplify the model complexity for future use in control and optimisation, the 10-step Trapezoidal rule (Eq. 12) is applied to eliminate the spatial dimension and the reactor is assumed to be a column with a square cross section. The area of the square is equal to that of the original circle, giving a width of 4.4 cm. This simplification was demonstrated to yield high accuracy in recent studies (del Rio-Chanona et al. 2017; del Rio-Chanona, Zhang, et al. 2015)

$$u_m(I) = \frac{u_M}{20} \cdot \sum_{n=1}^{9} \left(\frac{I_{i=0}}{I_{i=0} + k_s + \frac{I_{i=0}^2}{k_i}} + 2 \cdot \frac{I_{i=\frac{n \cdot L}{10}}}{I_{i=\frac{n \cdot L}{10}} + k_s + \frac{I_{i=\frac{n \cdot L}{10}}^2}{k_i}} + \frac{I_{i=L}}{I_{i=L} + k_s + \frac{I_{i=L}^2}{k_i}} \right) \quad (12)$$

where I_i is local light intensity at a distance of $i = \frac{n \cdot L}{10}$ from the reactor exposure surface.

2.3 Parameter estimation

Due to the high complexity of the dynamic model, it is vital to employ a robust parameter estimation method to identify the model parameter values in this study. Unreliable values can severely prevent the applicability of the dynamic model for real-time bioprocess control and optimisation. Therefore, a nonlinear least-squares optimisation problem is formulated. A high order orthogonal collocation method over finite elements in time is chosen to discretise and transform the current model into a nonlinear programming problem (NLP). The optimal values of model parameters are estimated by solving the NLP using IPOPT, the state-of-the-art interior point nonlinear optimisation solver (Wächter and Biegler 2005). This parameter estimation procedure is programmed in the Python optimisation environment Pyomo (Hart et al. 2012). Once the parameters are estimated, the model's simulation results are calculated in Mathematica® 10.

2.4 Sensitivity analysis

Sensitivity analysis was developed to estimate the effect of model parameters on the system performance, and has been widely used to identify the most influential parameters that affect

the process dynamics (Fouchard et al. 2009). A normalised sensitivity (S_i) is presented in Eq. 13. It measures the proportional change of the system's performance (c_i, *e.g.* FAME production) with respect to the proportional change of a model parameter (p_j). A positive sensitivity indicates that increasing p_j can result in an increase in c_i, whilst a negative sensitivity suggests that increasing p_j will diminish the system's performance. Moreover, a greater sensitivity also shows a more significant effect of the parameter on the system. In this research, sensitivity analysis is carried out in Mathematica® 10 to explore the effects of model kinetic parameters on both cells growth and FAME production.

$$S_i = \frac{\partial c_i / c_i}{\partial p_i / p_i} \tag{13}$$

3 Results and discussion

3.1 Results of parameter estimation

The values of the model parameters are listed in Table II, and the model fitting results are presented in Fig. 1 and Fig. 2. These figures show that our model provides a good representation of the underlying dynamic behaviour of the biosystem, indicating that the kinetic hypothesis and simplifications used in this study are valid. From Table II, it is observed that both the specific biomass decay rate and the bubble scattering coefficient equal 0, suggesting that they have negligible effects on the system. This can be attributed to the fact that in all the conducted experiments, biomass concentration kept increasing until the end of the study, disguising the effect of cell decay. Similarly, light attenuation is predominantly governed by cell absorption, and therefore the imperceptible impact of bubble scattering on light transmission is estimated to be 0.

The fluctuation of nitrogen quota and FAME yield at the beginning of the experiments in the two figures (Fig. 1(c), (d), and Fig. 2(c), (d)) can be attributed to the consumption of intracellularly stored nitrogen for cell growth and its subsequent replenishment through

nitrate uptake. At the start of the culture, the nitrogen quota (Fig. 1(c) and Fig. 2(c)) decreases significantly as it is consumed by algae biomass growth. This is followed the rapid uptake and conversion of culture nitrate into intracellularly stored nitrogen, resulting in the nitrogen quota to start to increase after a short period. However, as the total amount of nitrate in the culture is limited, once it is exhausted, the nitrogen quota keeps decreasing with the increasing algae biomass concentration. Similarly, as biolipid synthesis (hence FAME production) is severely inhibited under high nitrogen quota conditions (Mata, Martins, and Caetano 2010), the yield of FAME (Fig. 1(d) and Fig. 2(d)) increases when nitrogen quota drops, and decreases when nitrogen quota increases.

Confidence intervals are computed through the parameter estimation procedure. The covariance matrix for the estimated parameters is approximated by the inverse of the reduced Hessian at the optimal solution. Confidence intervals are then obtained from the trace of this approximated covariance matrix following standard procedures (del Rio-Chanona, Dechatiwongse, et al. 2015). However, as a result of the high nonlinearity and complexity of modelling metabolic kinetics, the assumption of computing the confidence intervals from the above framework may not hold. For this reason, the confidence intervals presented in Table II must be understood as theoretical values.

3.2 Sensitivity analysis results

The results from the sensitivity analysis are presented in Fig. 3. These show that for all state variables, a critical point exists around the 32^{nd} hour before and after which the sensitivity of variables with respect to the parameters changes dramatically. Based on the model, this point is estimated to be the time when the nitrate in the culture has been fully consumed. Thus, the sharp change of the parameter sensitivities indicates a rapid shift of metabolic reaction mechanisms inside biomass for its growth and synthesis of metabolites. Biomass concentration (Fig. 3(a)) and nitrogen quota (Fig. 3(c)) are found to be sensitive to the same

parameters, in particular u_M, k_q, k_s, and α, and their sensitivities are in a mild range of±0.8, suggesting a greater stability compared to nitrate concentration and FAME production.

Initially, whilst the nitrogen quota can be replenished by culture nitrate, both biomass concentration and nitrogen quota are predominantly governed by the light intensity (k_s, α) and the maximum specific growth rate (u_M). As u_M represents the maximum growth rate that cells can reach under nutrient sufficient conditions, it is expected that higher values of u_M correspond to faster cell growth, resulting in denser biomass concentrations. Similarly, a reduced algal biomass absorption coefficient (α) results in an increase in the local light intensity experienced by the cells, whilst a lower light saturation term (k_s) suggests that the light capacity for cells to grow is lower. Hence, biomass shows positive sensitivity to u_M and negative sensitivities to α and k_s. As higher biomass growth rates correspond to higher nitrogen quota consumption rates, it is unsurprising that the sensitivity of nitrogen quota with respect to these parameters is opposite in sign to that of biomass concentration.

Furthermore, nitrogen quota is highly sensitive to u_N which reflects how rapidly the cells can absorb nitrate and replenish their intracellular nitrogen storage. Consequently, once the culture nitrate is exhausted, the sensitivity of this term drops significantly and its effect on the nitrogen quota becomes negligible. At this point, the primary limiting factor for biomass growth is switched to the availability of intracellularly stored nitrogen. Therefore, k_q commences to show greater effects on both biomass concentration and nitrogen quota, whilst the sensitivity of u_M, k_s, and α keeps decreasing. As k_q represents the minimum nitrogen quota required by the cells to survive, a higher value of k_q suggests that cells can consume less of the stored nitrogen for growth and need a higher nitrogen quota for maintenance. Thus, it shows negative sensitivity to biomass concentration but positive sensitivity to nitrogen quota. In addition, Fig. 3(a) shows that the biomass concentration is insensitive to the light

inhibition term (k_i), suggesting that the current experiments were not subject to photoinhibition.

The sensitivity analysis reveals that both nitrate concentration and FAME production are highly sensitive to the model parameters (up to ±6.0), as a very small change (1%) of specific parameters, *e.g.* θ, γ, and u_N, can cause a dramatic change (up to 6%) on these variables. However, it is notable that the high sensitivities of these variables are attributed to different causes. The nitrate consumption rate only depends on a few parameters (u_N and K_N, Eq. 5), hence, the nitrate concentration is not substantially affected by microalgal metabolic reaction kinetics. This is also proven by its weak sensitivity (except u_N which directly represents the algal nitrate uptake rate) during the first 20 hours (shown in Fig. 3(b)) whilst nitrate is still available in the culture. Subsequently, as the nitrate concentration approaches 0, its sensitivity diverges sharply. However, this phenomenon is more probably caused by mathematical noise (*i.e.* $\partial N/N \to \infty$ when $N \to 0$, based on the definition of sensitivity, Eq. 13) instead of a biological reason.

In contrast, the sensitivities of FAME can be attributed to its complicated synthesis mechanisms. As biolipids constitute between 10% and 45% wt biomass, its production can be affected by the same factors that influence biomass growth. Therefore, from Fig. 3(d) it is found that the trends of the sensitivities of FAME with respect to both u_M and α are equal to those for biomass concentration. In addition, as biolipid can be converted to other metabolites and its consumption rate is proportional to the nitrate uptake rate, it is easy to see that u_N has a negative impact on FAME production when the culture is nitrate available (shown in Fig. 3(d)). Moreover, based on Eq. 8, θ and γ can be considered as the reaction kinetic constants for FAME synthesis and consumption, respectively. Thus, as presented in Fig. 3(d), these two parameters possess the highest sensitivities to FAME production, and become particularly

influential when the culture nitrate concentration approaches 0 and biolipid starts to accumulate.

Overall, the current sensitivity analysis demonstrates that the synthesis of FAME is more sensitive to the underlying biochemical reaction kinetics and experimental operating conditions than biomass growth or nitrogen quota accumulation,. Hence, in order to improve FAME production, it is vital to implement advanced process optimisation strategies which guarantee optimal cultivation conditions for FAME synthesis.

3.3 Limiting factors for FAME synthesis

Recent studies have concluded that light attenuation is one of the primary limiting factors for biomass cultivation and bioproduct production (D. Zhang et al. 2015; Béchet, Shilton, and Guieysse 2013). Similar results are obtained in the present work. Fig. 4(a) shows that over the course of the cultivation an increase in biomass concentration causes the local light intensity in the PBR to decrease rapidly, resulting in the majority of the reactor volume to be immersed in the dark zone where cells cannot grow (local growth rate drops to 0, shown in Fig. 4(b)). Both the local biomass growth rate and FAME production rate decrease with increasing biomass concentration inside the light zone where algal cells can receive illumination for their growth (Fig. 4(b) and Fig. 4(c)). This is caused by light attenuation and lack of nitrogen quota.

As illustrated already in the model construction section (Eq. 7), the synthesis of biolipid requires both illumination and nitrogen quota. During the initial experimental period when nitrate is still available, local light intensity is the primary limiting factor for biolipid synthesis. For example, at a biomass concentration of 0.7 g L^{-1}, the local biolipid synthesis rate decreases along the light transmission direction, indicating that light attenuation limits its production (Fig. 4(c)). However, after nitrate is consumed, the nitrogen quota decreases significantly in order to maintain the rapid growth of biomass (Fig. 4(b), x-axis between 0

and 0.01). As biolipid synthesis rate is proportional to nitrogen quota, its synthesis rate is also reduced dramatically (Fig. 4(c)) even when there is sufficient light for biomass growth (Fig. 4(a) and Fig. 4(b), x-axis in between 0 to 0.01). This clearly suggests that the primary limiting factor for FAME production has been switched to nitrogen quota. Similarly, because biomass growth is also related to nitrogen quota, the lack of nitrogen quota also causes a lower cell growth rate when biomass concentration increases from 1.5 g L^{-1} to 2.5 g L^{-1} as shown in Fig. 4(b).

Furthermore, based on the current simulation result, the effect of light intensity and nitrogen quota on FAME production is presented in Fig. 4(d). This shows, that the FAME production rate always increases with increasing nitrogen quota, whilst an optimal value exists for light intensity as intense illumination can damage the essential proteins for algal photosynthesis and carbon fixation. Based on the model, the optimal light intensity is identified to be 96 μmol m^{-2} s^{-1}, falling within the range of optimal light intensities reported in other publications (D. Zhang et al. 2015). In addition, attention should be paid to the fact that both the local biomass growth rate and the FAME production rate shown in Fig. 4 represent instantaneous values, as the location of individual algal cells change continuously as a result of mixing. Hence, cells at different locations in the reactor share the same average growth rate and biolipid synthesis rate over time.

3.4 Model predictive capability validation

To estimate the optimal operating conditions for long-term bioprocess optimisation, besides accurately representing a known experiment, the model must possess great predictive capability when simulating unknown processes. For this reason, the predictive capability of the constructed model is investigated through two scenarios. In the first scenario, the model is used to predict the dynamic performance of a continuous illumination batch experiment lasting for 11 days (252 hours). In the second scenario, the model is applied to predict a

light/dark cycle batch experiment lasting for one week (168 hours). It is worth emphasising that due to the frequent change of light intensity, the second system becomes more complex and has a higher uncertainty compared to the first scenario. Both light intensity and initial nitrate concentration in these two experiments are different from those used for model construction. The detailed operating conditions of these experiments are listed in Table I.

Fig. 5 and Fig. 6 present the model prediction results. Specific to the light/dark (14h: 10h) cycle experiment, biomass specific growth rate is slightly modified due to the significant impact of cell respiration on biomass growth in this case. The average specific biomass growth rate is assumed to be 85% of that under continuous illumination conditions (Edmundson and Huesemann 2015). The figures demonstrate that the current model is capable of accurately predicting the complex behaviour of long-term microalgal FAME production processes under different operating conditions, which indicates its great potential for future process control and optimisation applications. More importantly, as microalgae based bioprocesses are generally carried out under outdoor conditions for large scale production, it is impossible to provide continuous illumination for FAME production when scaling up this process.

During future research, we will implement an online optimal control strategy which measures experimental parameters (*e.g.* nutrients and biomass concentration) in real-time, whilst the model is adjusted to best represent the system under consideration. Through this framework, optimal inputs (*e.g.* nutrient supply) can be computed and implemented in an ongoing process (*e.g.* economic model predictive control). However, for this strategy to be possible, the model must be able to display solid predictive capabilities and robustness to model parameters. These have been clearly shown in the work above, particularly regarding to the second scenario, demonstrating its applicability for future process real-time optimisation and scale-up design.

Conclusions

In the current research, a mathematical model was constructed to simulate the growth and biodiesel production from *Nannochloropsis oceanica*. By conducting a sensitivity analysis, it was found that biolipid synthesis is more sensitive to the operating parameters of the system than cell growth. Therefore, in order to maintain high biomass concentrations as well as high biolipid productivities in long-term processes, it is vital to precisely estimate the nitrogen dosing requirements and implement advanced process optimisation strategies. This emphasises the importance of constructing a highly accurate dynamic model characterised by good predictive capability as presented in this study. During future work, this model will be incorporated into a state-of-the-art process real-time control framework, such as economic model predictive control, to optimise the operating conditions for semi-continuous (fed-batch) and continuous biodiesel production processes, in particularly under light/dark cycle circumstances.

Acknowledgement

This project is granted by EPSRC project (EP/P016650/1, P65332) and Natural Science Foundation of China (No. 21576253).

References

Adesanya, Victoria O., Matthew P. Davey, Stuart A. Scott, and Alison G. Smith. 2014. "Kinetic Modelling of Growth and Storage Molecule Production in Microalgae under Mixotrophic and Autotrophic Conditions." *Bioresource Technology* 157 (April): 293–304. doi:10.1016/j.biortech.2014.01.032.

Béchet, Quentin, Andy Shilton, and Benoit Guieysse. 2013. "Modeling the Effects of Light and Temperature on Algae Growth: State of the Art and Critical Assessment for Productivity Prediction during Outdoor Cultivation." *Biotechnology Advances* 31 (8). Elsevier Inc.: 1648–63. doi:10.1016/j.biotechadv.2013.08.014.

Bernard, Olivier, Francis Mairet, and Benoît Chachuat. 2015. “Modelling of Microalgae Culture Systems with Applications to Control and Optimization.” In , 59–87. doi:10.1007/10_2014_287.

Brennan, Liam, and Philip Owende. 2010. “Biofuels from microalgae—A Review of Technologies for Production, Processing, and Extractions of Biofuels and Co-Products.” *Renewable and Sustainable Energy Reviews* 14 (2). Elsevier Ltd: 557–77. doi:10.1016/j.rser.2009.10.009.

Cakmak, Turgay, Pinar Angun, Yunus Emre Demiray, Alper Devrim Ozkan, Zeynep Elibol, and Turgay Tekinay. 2012. “Differential Effects of Nitrogen and Sulfur Deprivation on Growth and Biodiesel Feedstock Production of Chlamydomonas Reinhardtii.” *Biotechnology and Bioengineering* 109 (8): 1947–57. doi:10.1002/bit.24474.

Chi, Lei, Changhong Yao, Xupeng Cao, and Song Xue. 2016. “Coordinated Regulation of Nitrogen Supply Mode and Initial Cell Density for Energy Storage Compounds Production with Economized Nitrogen Utilization in a Marine Microalga Isochrysis Zhangjiangensis.” *Bioresource Technology* 200 (January): 598–605. doi:10.1016/j.biortech.2015.10.059.

Converti, Attilio, Alessandro A. Casazza, Erika Y. Ortiz, Patrizia Perego, and Marco Del Borghi. 2009. “Effect of Temperature and Nitrogen Concentration on the Growth and Lipid Content of Nannochloropsis Oculata and Chlorella Vulgaris for Biodiesel Production.” *Chemical Engineering and Processing: Process Intensification* 48 (6): 1146–51. doi:10.1016/j.cep.2009.03.006.

Edmundson, Scott J., and Michael H. Huesemann. 2015. “The Dark Side of Algae Cultivation: Characterizing Night Biomass Loss in Three Photosynthetic Algae, Chlorella Sorokiniana, Nannochloropsis Salina and Picochlorum Sp.” *Algal Research* 12 (November): 470–76. doi:10.1016/j.algal.2015.10.012.

481 Eroglu, Ela, and Anastasios Melis. 2010. “Extracellular Terpenoid Hydrocarbon Extraction
482 and Quantitation from the Green Microalgae Botryococcus Braunii Var. Showa.”
483 *Bioresource Technology* 101 (7). Google Patents: 2359–66.
484 doi:10.1016/j.biortech.2009.11.043.
485 Fouchard, S, J Pruvost, B Degrenne, M Titica, and J Legrand. 2009. “Kinetic Modeling of
486 Light Limitation and Sulfur Deprivation Effects in the Induction of Hydrogen
487 Production with Chlamydomonas Reinhardtii: Part I. Model Development and
488 Parameter Identification.” *Biotechnology and Bioengineering* 102 (1): 232–77.
489 doi:10.1002/bit.22034.
490 Gnansounou, Edgard, and Jegannathan Kenthorai Raman. 2016. “Life Cycle Assessment of
491 Algae Biodiesel and Its Co-Products.” *Applied Energy* 161 (January): 300–308.
492 doi:10.1016/j.apenergy.2015.10.043.
493 Hart, William E., Carl Laird, Jean-Paul Watson, and David L. Woodruff. 2012. *Pyomo –
494 Optimization Modeling in Python*. Vol. 67. Springer Optimization and Its Applications.
495 Boston, MA: Springer US. doi:10.1007/978-1-4614-3226-5.
496 Keymer, Philip C., Steven Pratt, and Paul A. Lant. 2013. “Development of a Novel
497 Electrochemical System for Oxygen Control (ESOC) to Examine Dissolved Oxygen
498 Inhibition on Algal Activity.” *Biotechnology and Bioengineering* 110 (9): 2405–11.
499 doi:10.1002/bit.24905.
500 Li, Yanqun, Mark Horsman, Bei Wang, Nan Wu, and Christopher Q. Lan. 2008. “Effects of
501 Nitrogen Sources on Cell Growth and Lipid Accumulation of Green Alga Neochloris
502 Oleoabundans.” *Applied Microbiology and Biotechnology* 81 (4): 629–36.
503 doi:10.1007/s00253-008-1681-1.
504 Liu, Jiao, Yanan Liu, Haitao Wang, and Song Xue. 2015. “Direct Transesterification of Fresh
505 Microalgal Cells.” *Bioresource Technology* 176 (January): 284–87.

506 doi:10.1016/j.biortech.2014.10.094.
507 Mata, Teresa M., António A. Martins, and Nidia. S. Caetano. 2010. “Microalgae for
508 Biodiesel Production and Other Applications: A Review.” *Renewable and Sustainable*
509 *Energy Reviews* 14 (1): 217–32. doi:10.1016/j.rser.2009.07.020.
510 Matos, Cristina T., Luisa Gouveia, Ana Rita C. Morais, Alberto Reis, and Rafał Bogel-
511 Łukasik. 2013. “Green Metrics Evaluation of Isoprene Production by Microalgae and
512 Bacteria.” *Green Chem.* 15 (10): 2854–64. doi:10.1039/C3GC40997J.
513 Pan, Yanfei, Haibo Yang, Yingying Meng, Jiao Liu, Peili Shen, Peichun Wu, Xupeng Cao,
514 and Song Xue. 2016. “The Utilization of Natural Soda Resource of Ordos in the
515 Cultivation of Nannochloropsis Oceanica.” *Bioresource Technology* 200 (January):
516 548–56. doi:10.1016/j.biortech.2015.10.068.
517 Park, Stephen, and Yebo Li. 2015. “Integration of Biological Kinetics and Computational
518 Fluid Dynamics to Model the Growth of Nannochloropsis Salina in an Open Channel
519 Raceway.” *Biotechnology and Bioengineering* 112 (5): 923–33. doi:10.1002/bit.25509.
520 Purkayastha, Jubilee, Ajitabh Bora, Hemanta Kumar Gogoi, and Lokendra Singh. 2017.
521 “Growth of High Oil Yielding Green Alga Chlorella Ellipsoidea in Diverse Autotrophic
522 Media, Effect on Its Constituents.” *Algal Research* 21 (January): 81–88.
523 doi:10.1016/j.algal.2016.11.009.
524 Rio-Chanona, Ehecatl Antonio del, Nur rashid Ahmed, Dongda Zhang, Yinghua Lu, and
525 Keju Jing. 2017. “Kinetic Modeling and Process Analysis for Desmodesmus Sp. Lutein
526 Photo-Production.” *AIChE Journal* 63 (7): 2546–54. doi:10.1002/aic.15667.
527 Rio-Chanona, Ehecatl Antonio del, Pongsathorn Dechatiwongse, Dongda Zhang, Geoffrey C.
528 Maitland, Klaus Hellgardt, Harvey Arellano-Garcia, and Vassilios S. Vassiliadis. 2015.
529 “Optimal Operation Strategy for Biohydrogen Production.” *Industrial & Engineering*
530 *Chemistry Research* 54 (24): 6334–43. doi:10.1021/acs.iecr.5b00612.

Rio-Chanona, Ehecatl Antonio del, Dongda Zhang, and Vassilios S. Vassiliadis. 2016. "Model-Based Real-Time Optimisation of a Fed-Batch Cyanobacterial Hydrogen Production Process Using Economic Model Predictive Control Strategy." *Chemical Engineering Science* 142 (March): 289–98. doi:10.1016/j.ces.2015.11.043.

Rio-Chanona, Ehecatl Antonio del, Dongda Zhang, Youping Xie, Emmanuel Manirafasha, and Keju Jing. 2015. "Dynamic Simulation and Optimization for Arthrospira Platensis Growth and C-Phycocyanin Production." *Industrial & Engineering Chemistry Research* 54 (43): 10606–14. doi:10.1021/acs.iecr.5b03102.

Schenk, Peer M., Skye R. Thomas-Hall, Evan Stephens, Ute C. Marx, Jan H. Mussgnug, Clemens Posten, Olaf Kruse, and Ben Hankamer. 2008. "Second Generation Biofuels: High-Efficiency Microalgae for Biodiesel Production." *BioEnergy Research* 1 (1): 20–43. doi:10.1007/s12155-008-9008-8.

Scott, Stuart A, Matthew P Davey, John S Dennis, Irmtraud Horst, Christopher J Howe, David J Lea-Smith, and Alison G Smith. 2010. "Biodiesel from Algae: Challenges and Prospects." *Current Opinion in Biotechnology* 21 (3): 277–86. doi:10.1016/j.copbio.2010.03.005.

Sharma, Kalpesh K., Holger Schuhmann, and Peer M. Schenk. 2012. "High Lipid Induction in Microalgae for Biodiesel Production." *Energies* 5 (12): 1532–53. doi:10.3390/en5051532.

Sheehan, John, Terri Dunahay, John R Benemann, and Paul Roessler. 1998. "A Look Back at the US Department of Energy's Aquatic Species Program: Biodiesel from Algae." *US Department of Energy (US DoE) Office of Fuels Development, Prepared by National Renewable Energy Laboratory (NREL)*. National Renewable Energy Laboratory Golden, CO.

Wächter, A., and L. T. Biegler. 2005. *On the Implementation of an Interior-Point Filter Line-*

556 *Search Algorithm for Large-Scale Nonlinear Programming*. *Mathematical*
557 *Programming*. Vol. 106. doi:10.1007/s10107-004-0559-y.
558 Wang, Yong-Zhong, Patrick C. Hallenbeck, Gustavo B. Leite, Kiran Paranjape, and Dan-Qun
559 Huo. 2016. "Growth and Lipid Accumulation of Indigenous Algal Strains under
560 Photoautotrophic and Mixotrophic Modes at Low Temperature." *Algal Research* 16
561 (June): 195–200. doi:10.1016/j.algal.2016.03.017.
562 Wen, Xiaobin, Kui Du, Zhongjie Wang, Xinan Peng, Liming Luo, Huanping Tao, Yan Xu,
563 Dan Zhang, Yahong Geng, and Yeguang Li. 2016. "Effective Cultivation of Microalgae
564 for Biofuel Production: A Pilot-Scale Evaluation of a Novel Oleaginous Microalga
565 Graesiella Sp. WBG-1." *Biotechnology for Biofuels* 9 (1): 123. doi:10.1186/s13068-016-
566 0541-y.
567 Yao, Changhong, Jiangning Ai, Xupeng Cao, Song Xue, and Wei Zhang. 2012. "Enhancing
568 Starch Production of a Marine Green Microalga Tetraselmis Subcordiformis through
569 Nutrient Limitation." *Bioresource Technology* 118 (August): 438–44.
570 doi:10.1016/j.biortech.2012.05.030.
571 Yoo, Chan, Hyun-Joon La, Sun-Chang Kim, and Hee-Mock Oh. 2015. "Simple Processes for
572 Optimized Growth and Harvest of Ettlia Sp. by pH Control Using CO2 and Light
573 Irradiation." *Biotechnology and Bioengineering* 112 (2): 288–96. doi:10.1002/bit.25362.
574 Yoo, Sung Jin, Jung Hun Kim, and Jong Min Lee. 2014. "Dynamic Modelling of
575 Mixotrophic Microalgal Photobioreactor Systems with Time-Varying Yield Coefficient
576 for the Lipid Consumption." *Bioresource Technology* 162. Elsevier Ltd: 228–35.
577 doi:10.1016/j.biortech.2014.03.128.
578 Zhang, D., P. Dechatiwongse, E.A. del Rio-Chanona, G.C. Maitland, K. Hellgardt, and V.S.
579 Vassiliadis. 2015. "Modelling of Light and Temperature Influences on Cyanobacterial
580 Growth and Biohydrogen Production." *Algal Research* 9.

doi:10.1016/j.algal.2015.03.015.

Zhang, Dongda, Ehecatl Antonio Del-Rio Chanona, Vassilios S Vassiliadis, and Bojan Tamburic. 2015. “Analysis of Green Algal Growth via Dynamic Model Simulation and Process Optimization.” *Biotechnology and Bioengineering* 112 (10): 2025–39. doi:10.1002/bit.25610.

Zhang, Dongda, Minxi Wan, Ehecatl Antonio del Rio-Chanona, Jianke Huang, Weiliang Wang, Yuanguang Li, and Vassilios S. Vassiliadis. 2016. “Dynamic Modelling of Haematococcus Pluvialis Photoinduction for Astaxanthin Production in Both Attached and Suspended Photobioreactors.” *Algal Research* 13 (12): 69–78. doi:10.1016/j.algal.2015.11.019.

Zhu, C. J., and Y. K. Lee. 1997. “Determination of Biomass Dry Weight of Marine Microalgae.” *Journal of Applied Phycology* 9 (2): 189–94. doi:10.1023/A:1007914806640.

596 Table I: Operating conditions of current experiments

	Experiment 1	Experiment 2
Incident light intensity, μmol m^{-2} s^{-1}	80	160
Initial nitrate concentration, mg L^{-1}	35.0	24.6
Initial biomass concentration, g L^{-1}	0.18	0.17
Initial FAME yield, wt%	12.0	11.2
Initial nitrogen quota, wt%	8.0	7.9
Initial chlorophyll fluorescence	0.561	0.555
Operation time, day	11	11
	Experiment 3	Experiment 4
Incident light intensity, μmol m^{-2} s^{-1}	120	140, (light/dark (14h:10h))
Initial nitrate concentration, mg L^{-1}	46.8	15.2
Initial biomass concentration, g L^{-1}	0.18	0.18
Initial FAME yield, wt%	12.0	11.7
Initial nitrogen quota, wt%	8.0	8.2
Initial chlorophyll fluorescence	0.561	0.571
Operation time, day	11	7

597

598

599

600

601 Table II: Model parameter estimation result

Parameter	Value	Parameter	Value
u_M, h^{-1}	0.359±0.014	θ	6.691±2.247
u_d, h^{-1}	0.0±0.000	γ	$(7.53±2.25)\times10^{-3}$
k_q, mg g^{-1}	1.963±0.283	ε	0.010±0.0004
u_N, mg g^{-1} h^{-1}	2.692±0.641	τ	1.376±0.139
K_N, mg L^{-1}	0.80±0.029	δ	9.904±3.013
k_s, μmol m^{-2} s^{-1}	91.2±1.727	φ	-0.456±0.011
k_i, μmol m^{-2} s^{-1}	100.0±0.290	β, m^{-1}	0.0±0.009
α, m^2 g^{-1}	196.4±21.6		

602

603

604

605

606 Figure 1: Comparison of model simulation results and real experimental data (Experiment 1).

607 Line: model simulation results, point: real experimental data. (a): biomass concentration; (b):

608 nitrate concentration; (c): nitrogen quota; (d): FAME yield; (e): chlorophyll fluorescence.

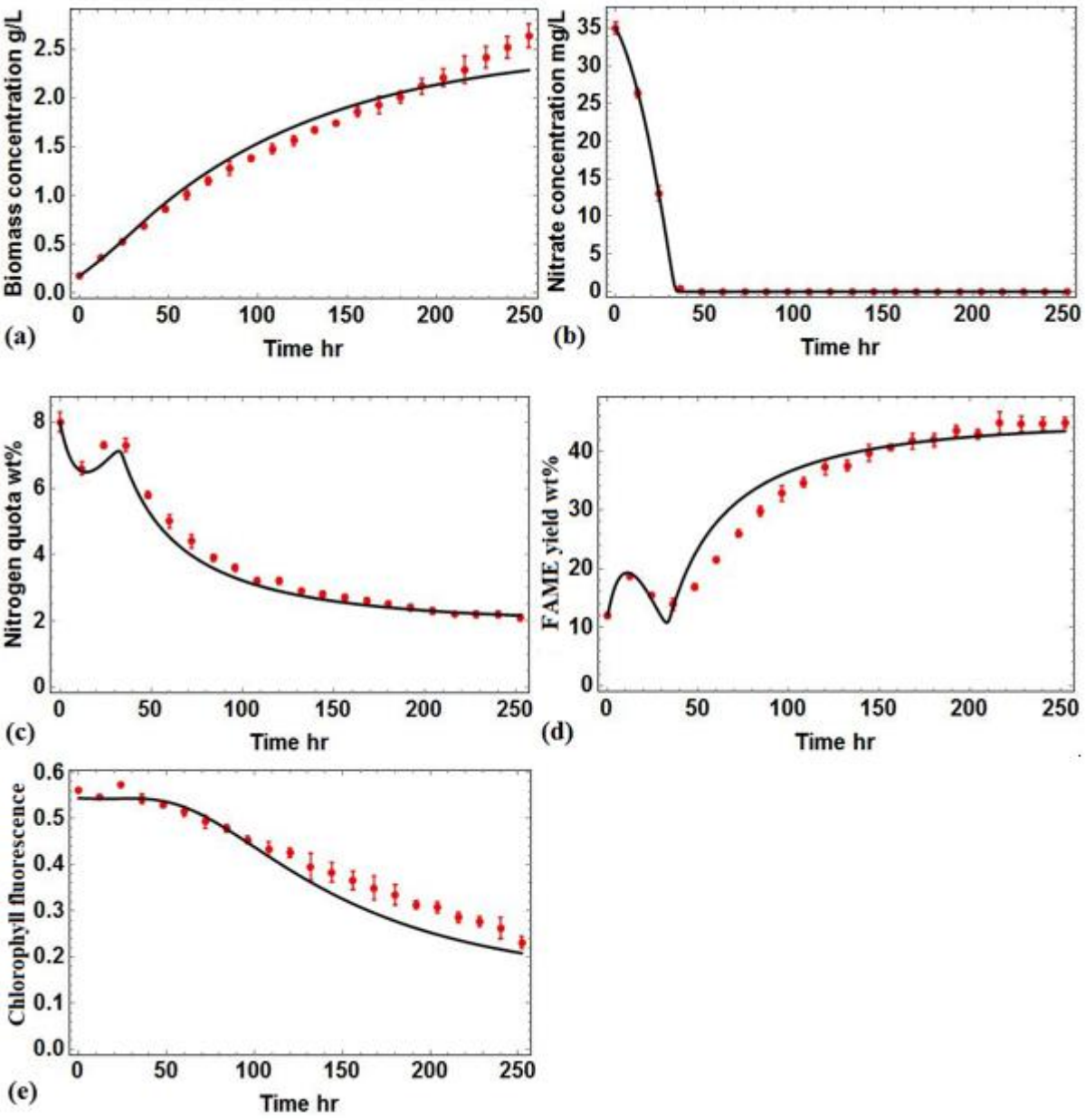

609

610

611 Figure 2: Comparison of model simulation results and real experimental data (Experiment 2).

612 Line: model simulation results, point: real experimental data. (a): biomass concentration; (b):

613 nitrate concentration; (c): nitrogen quota; (d): FAME yield; (e): chlorophyll fluorescence.

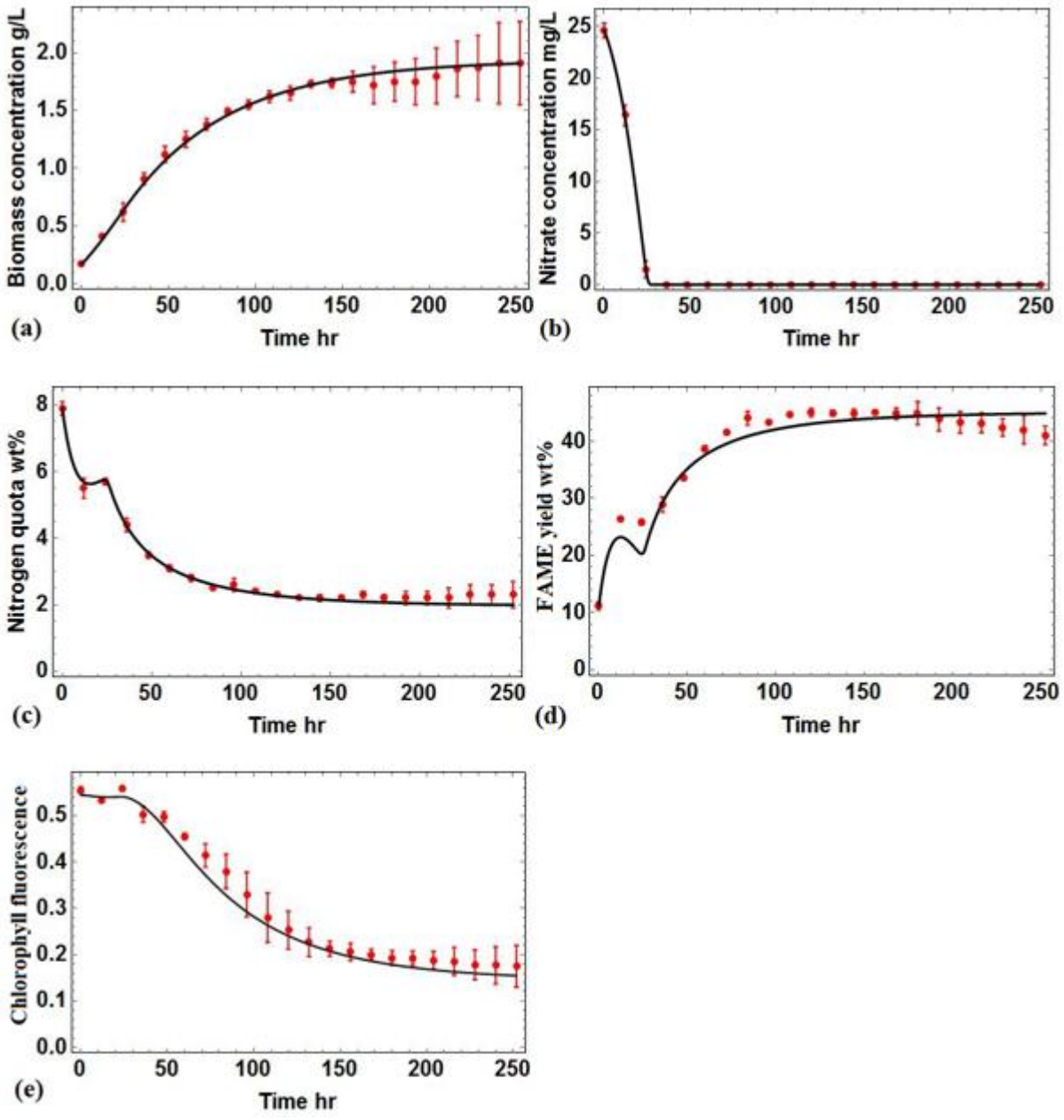

614

615

616

617

Figure 3: Sensitivity analysis of different variables on model parameters. (a): sensitivity of biomass concentration; (b): sensitivity of nitrate concentration; (c): sensitivity of nitrogen quota; (d): sensitivity of FAME yield.

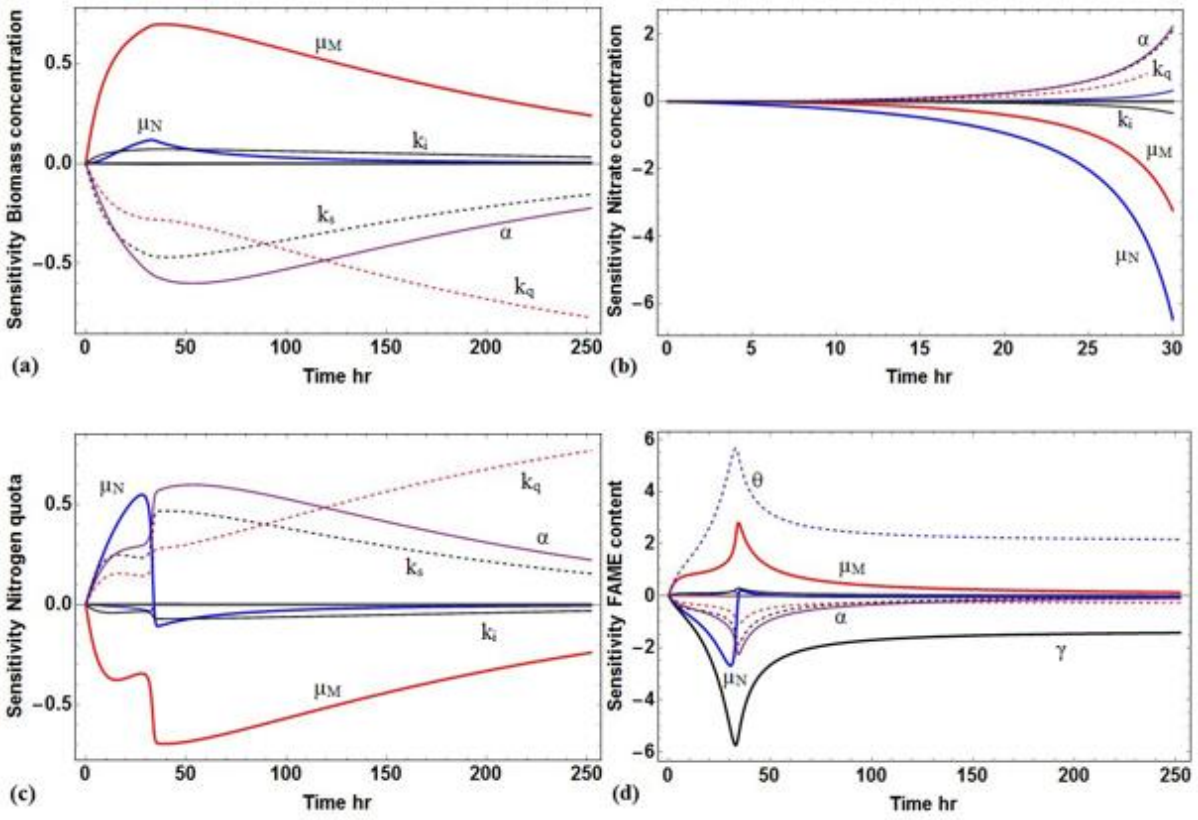

Figure 4: Effects of light attenuation and nitrogen quota on biomass growth and FAME production. (a): local light intensity; (b): local biomass growth rate; (c): local FAME production rate; (d): effect of light intensity and nitrogen quota on FAME production. Fig. 4(d) is obtained by Eq. 5, 8, 10, and 11, instead of the entire dynamic model.

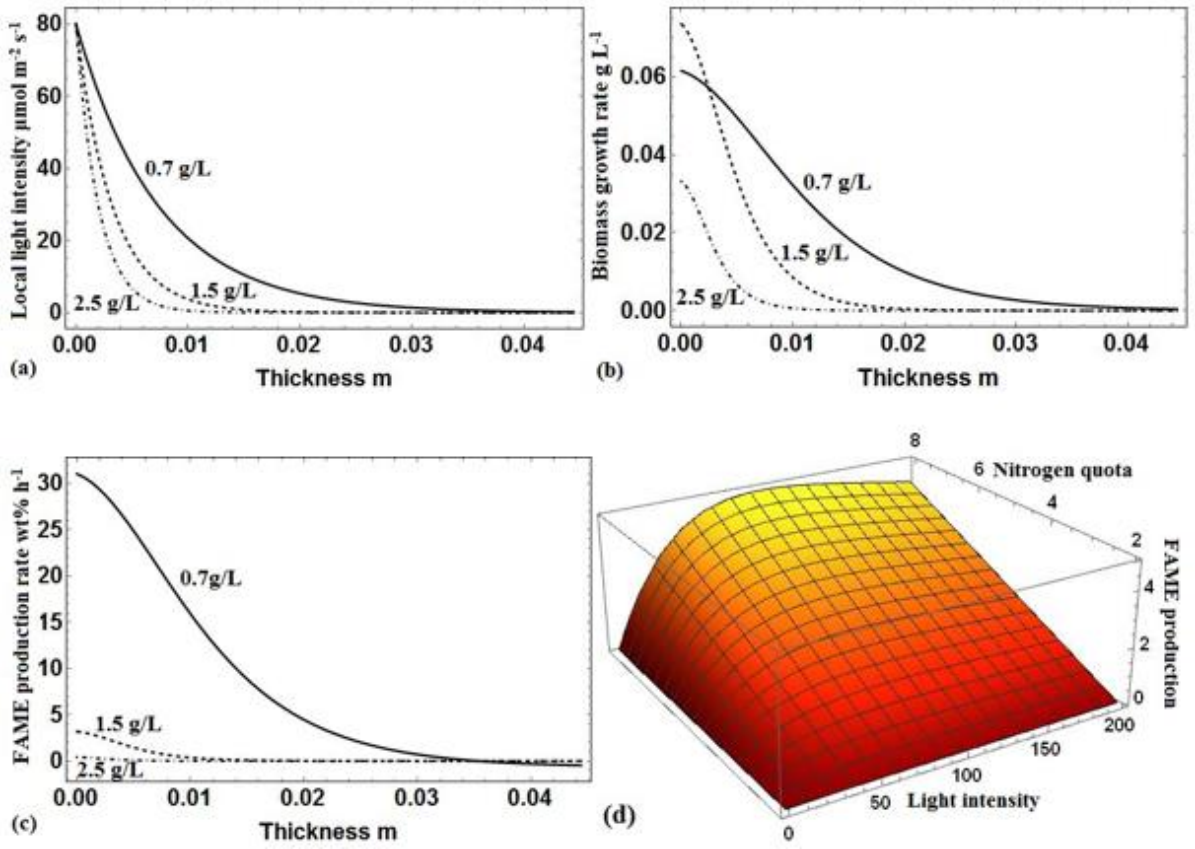

Figure 5: Comparison of model prediction results and real experimental data (Experiment 3). Line: model predication results, point: real experimental data. (a): biomass concentration; (b): nitrate concentration; (c): nitrogen quota; (d): FAME yield; (e): chlorophyll fluorescence.

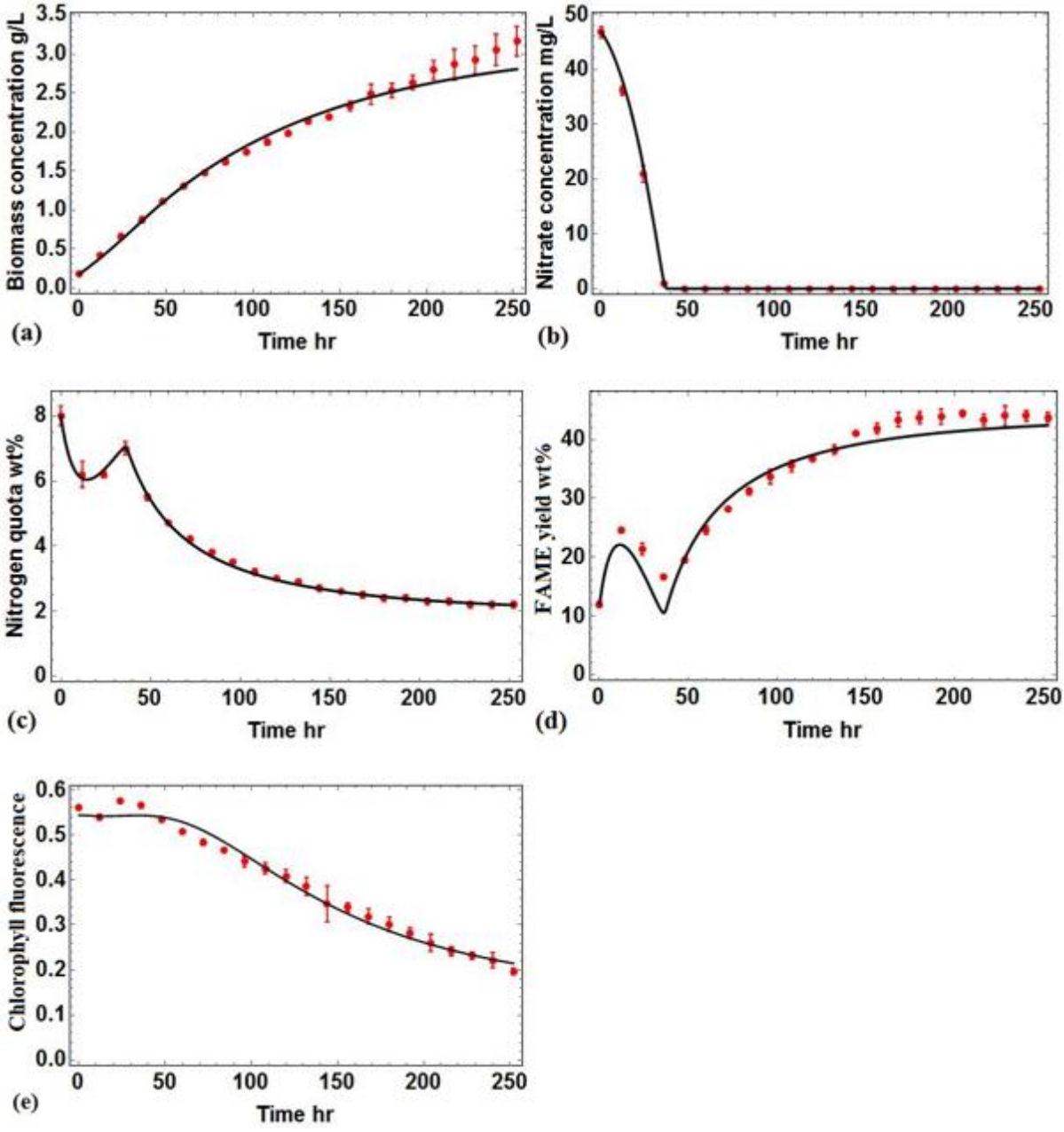

Figure 6: Comparison of model prediction results and real experimental data (Experiment 4). Line: model predication results, point: real experimental data. (a): biomass concentration; (b): nitrate concentration; (c): nitrogen quota; (d): FAME yield; (e): chlorophyll fluorescence; (f): incident light intensity.

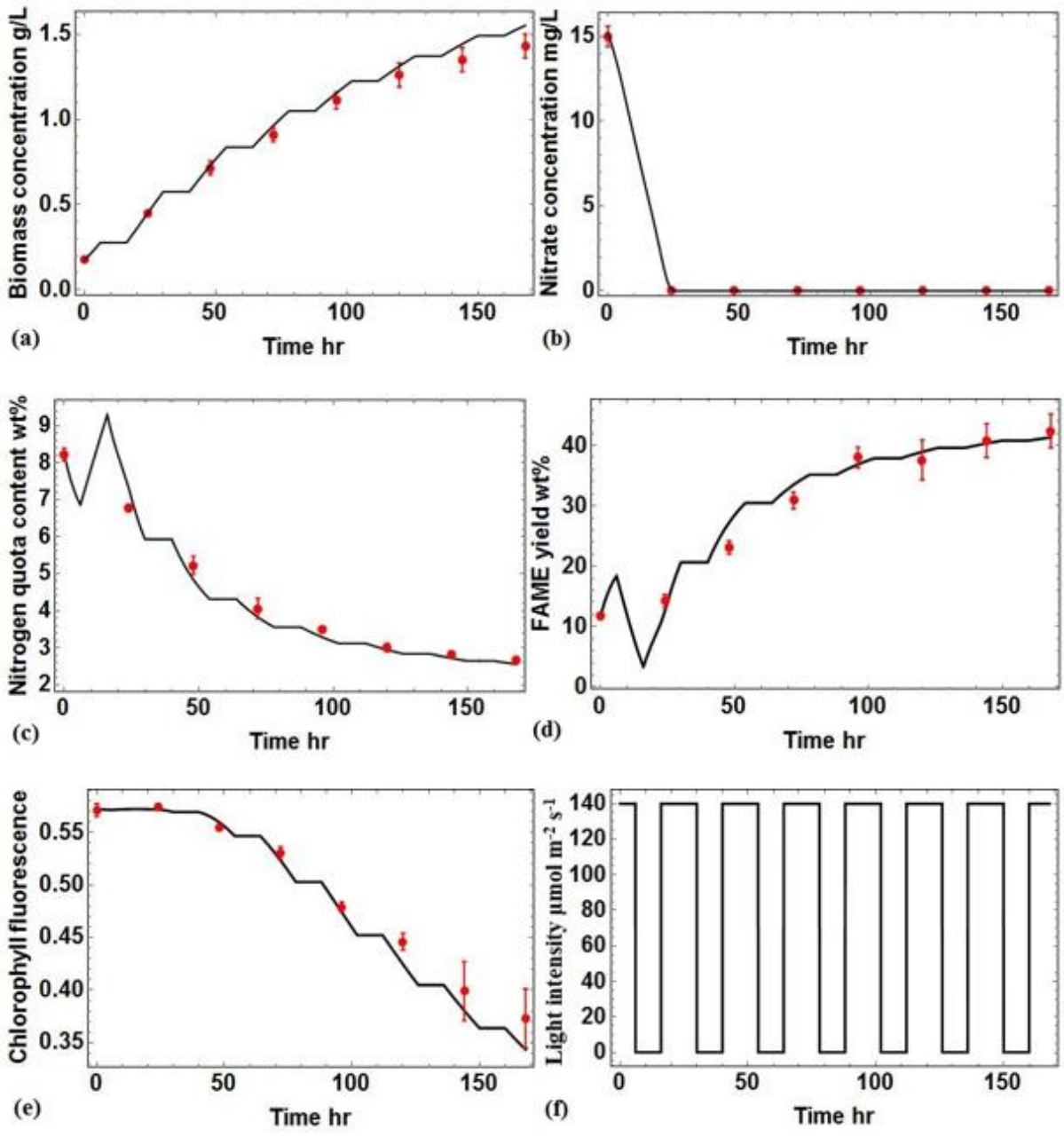

644 Graphical Table of Contents: A robust kinetic model was constructed to simulate the dynamic
645 behaviour of green microalgae biomass growth and biolipid (precursor of biodiesel)
646 production; correlation between chlorophyll fluorescence, an instantly measurable variable
647 and indicator of photosynthetic activity, and intracellular nitrogen content, which directly
648 affects biolipid synthesis rate, is quantified for the first time; through experimental
649 verification, the current model is characterised by a high level of predictive capability, and
650 the optimal light intensity for algal biomass growth and lipid synthesis is estimated.
651

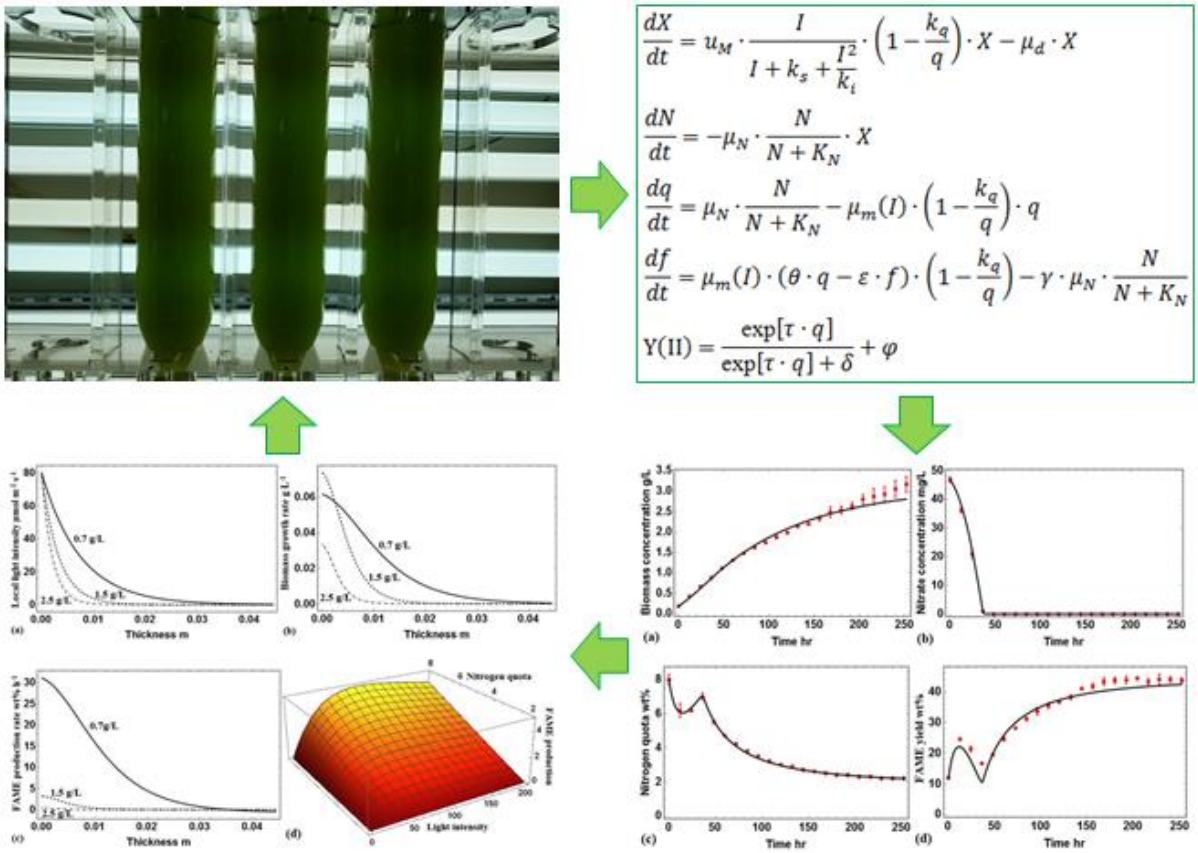

652

653